Electronic Supplementary Information

Bottom-up self-assembly of nano-netting cluster microspheres as high-performance lithium storage materials

Kyungbae Kim and Jae-Hun Kim*

School of Materials Science and Engineering, Kookmin University, Seoul 02707, Republic of Korea

* Corresponding author.

E-mail address: jaehunkim@kookmin.ac.kr (J.-H. Kim)

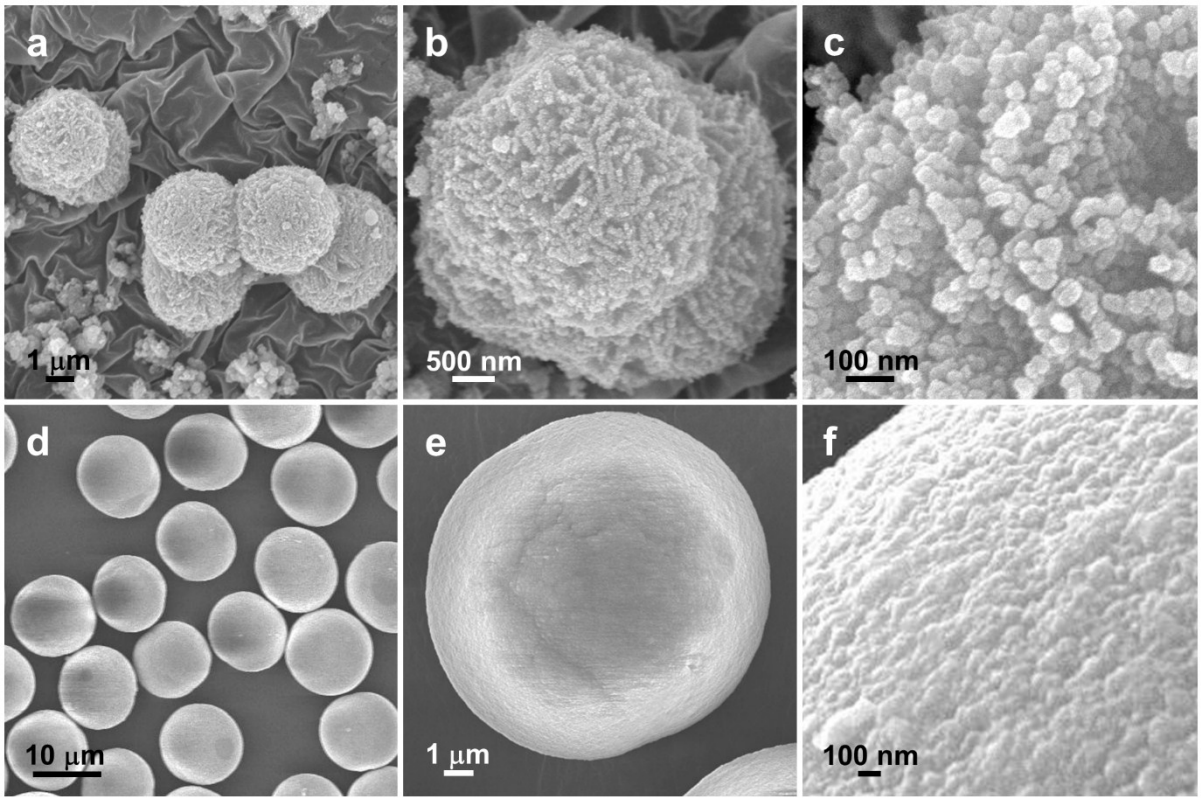

Fig. S1. FE-SEM images of separately synthesized (a–c) Nb_2O_5 nanoparticle clusters and (d–f) GeO_2 microspheres.

For a better understanding of the cluster microsphere formation process, we prepared the Nb_2O_5 and GeO_2 materials separately using the same solvothermal synthesis conditions. For the synthesis of Nb_2O_5, ammonium niobate(V) oxalate hydrate ($C_4H_4NNbO_9 \cdot xH_2O$; 10 mmol; Sigma Aldrich), a 2 M HCl solution, and Pluronic F-127 (Sigma Aldrich) were mixed in a beaker with ethyl alcohol (EtOH)/dimethylformamide (DMF) (volume ratio: 4:6) under sonication for 20 min. After stirring, the solution was transferred to a Teflon-lined steel reactor and heated to 200°C for 24 h. After this treatment, the resulting suspension was collected and cleaned several times using EtOH and deionized water in a centrifuge and dried at 65°C under vacuum. Subsequently, the as-prepared sample was heated to 600°C and

maintained in an Ar atmosphere for 2 h to crystallize the sample. For the GeO_2 material, the ammonium niobate(V) oxalate hydrate was replaced by germanium(IV) chloride ($GeCl_4$; 40 mmol, Alfa Aesar) without HCl solution.

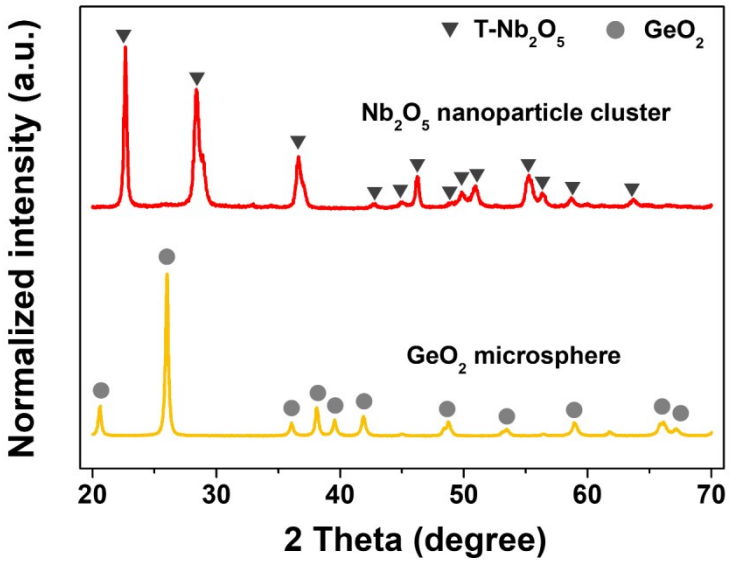

Fig. S2. XRD patterns of Nb_2O_5 nanoparticle clusters and GeO_2 microspheres.

The crystal structure of the synthesized Nb_2O_5 nanoparticle cluster was found to the orthorhombic (JCPDS No. 30-0873), as shown in Fig. S2. The diffraction peaks in the XRD pattern of the GeO_2 microspheres matched well with the crystal structure of hexagonal GeO_2 (JCPDS No. 36-1463).

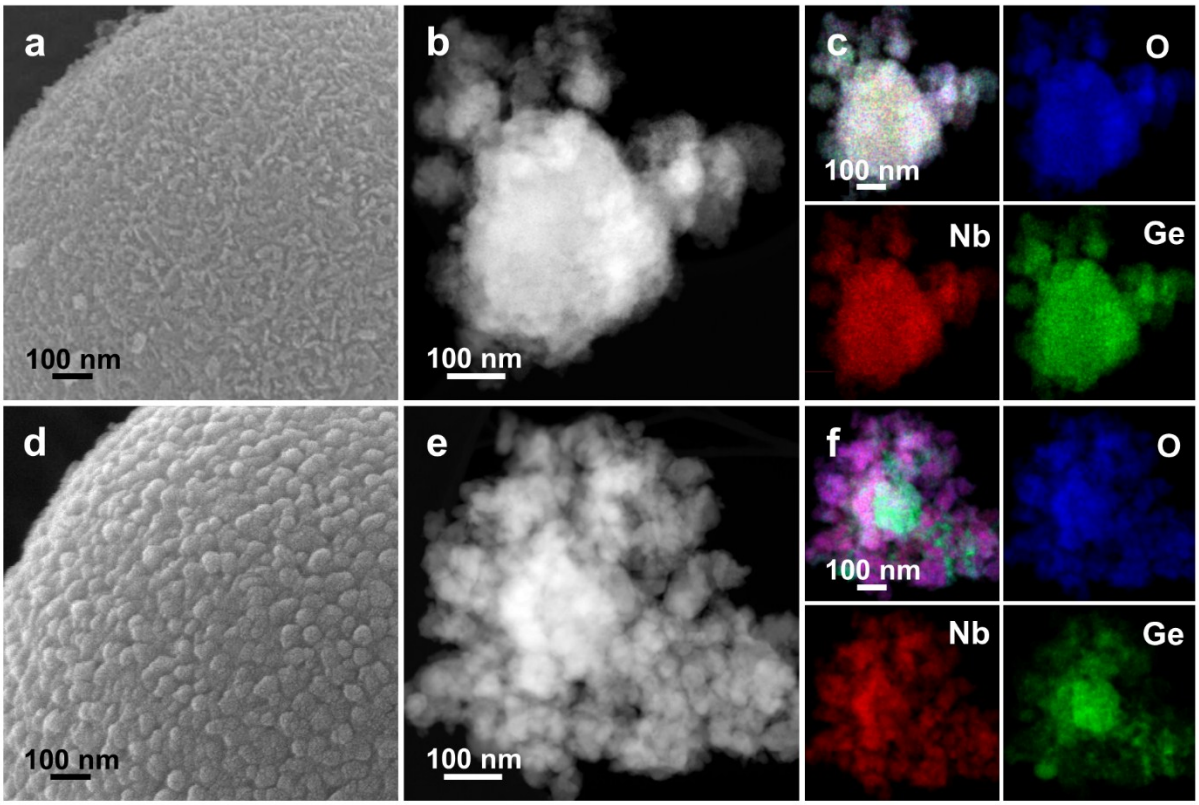

Fig. S3. FE-SEM and high-angle annular dark-field (HAADF) TEM images with corresponding EDS elemental mapping images showing the surface morphologies of the prepared samples. Each microsphere was mechanically ruptured to observe the individual components: (a–c) as-prepared NbO_x–GeO_x material and (d–f) heat-treated Nb_2O_5–Ge/GeO_2 cluster microspheres.

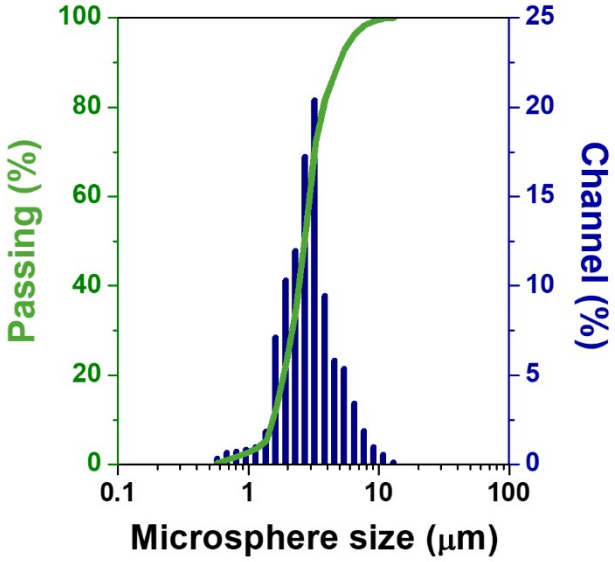

Fig. S4. Particle size distribution of the Nb_2O_5–Ge/GeO_2 cluster microspheres.

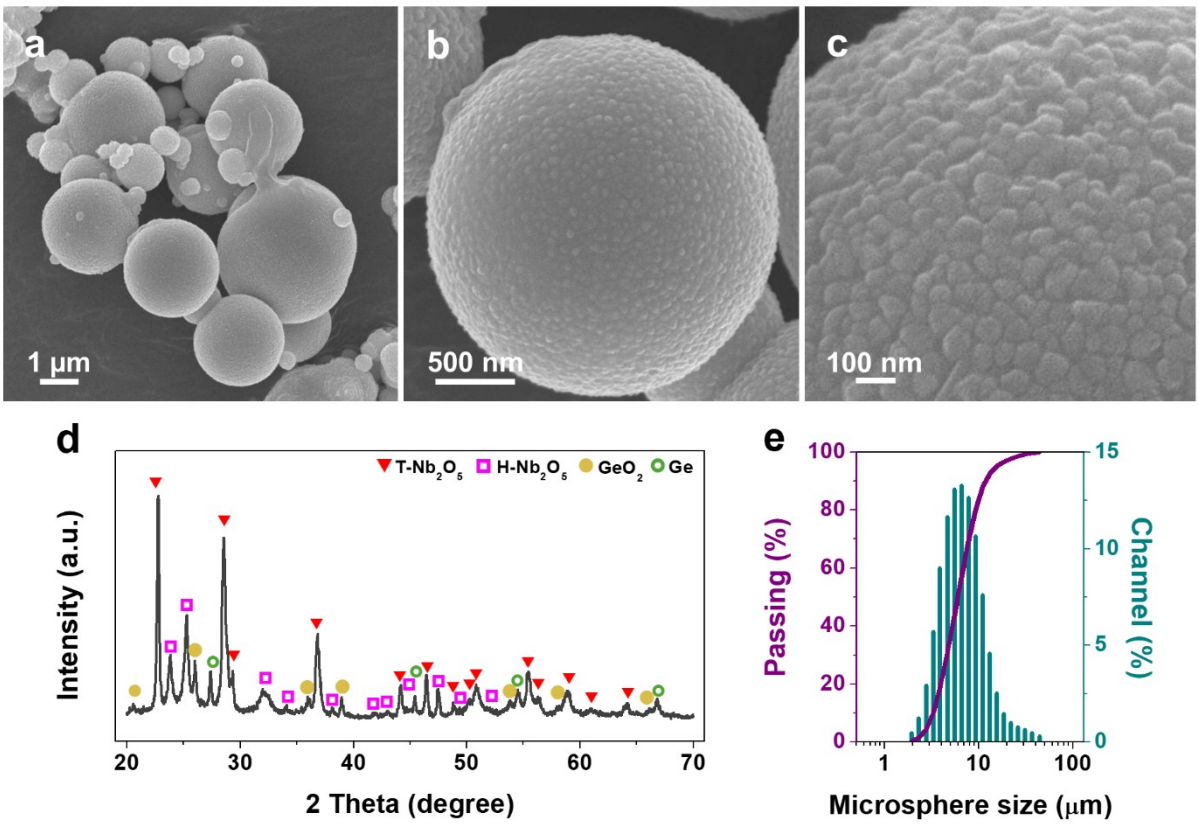

Fig. S5. For comparison, Nb_2O_5–Ge/GeO_2 cluster microspheres are synthesized without polyvinylpyrrolidone (PVP) as a capping agent: (a–c) FE-SEM images at various magnifications, (d) XRD pattern, and (e) particle size distribution. The average particle size is measured to be ~7 μm, which is bigger than the particles synthesized with PVP.

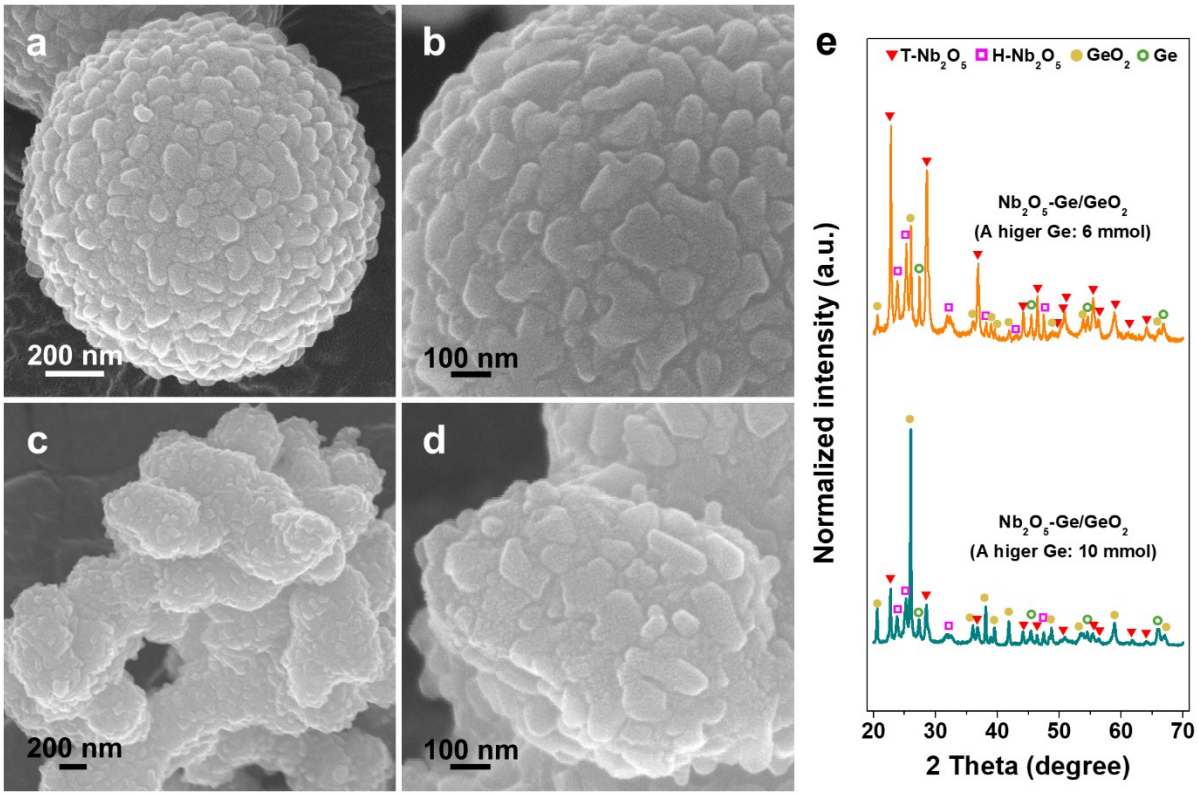

Fig. S6. (a and b) FE-SEM images of Nb_2O_5–Ge/GeO_2 cluster particles synthesized using a higher Ge precursor concentration (6 mmol), (c and d) saturated Ge/GeO_2 incorporation (10 mmol) in Nb_2O_5–Ge/GeO_2 particles, and (e) XRD patterns. It is evident that the cluster particle morphology and crystal structure are dependent on the ratio of Nb and Ge precursors as starting materials.

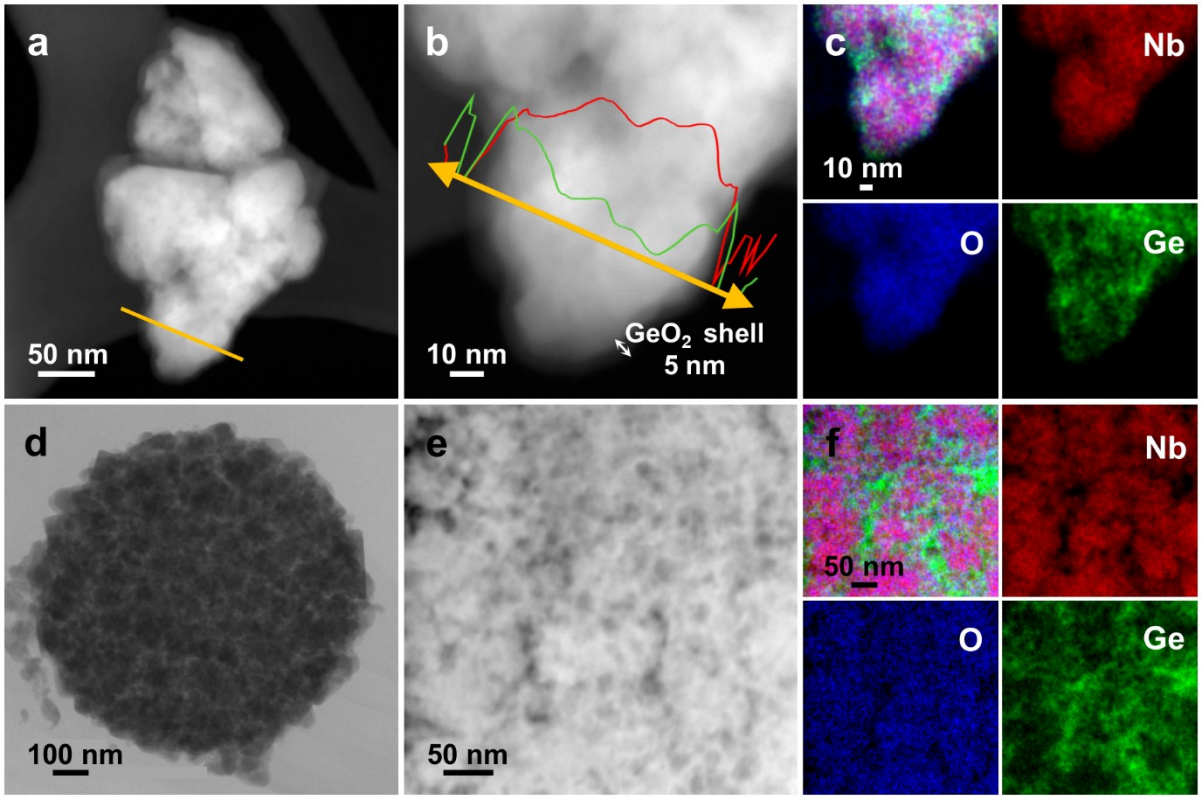

Fig. S7. (a) HAADF TEM image, EDS (b) line and (c) elemental mapping images, (d and e) cross-sectional TEM images at various magnifications, and (f) high-resolution EDS elemental mapping images of Nb_2O_5–Ge/GeO_2 cluster particles containing a higher Ge precursor concentration (6 mmol).

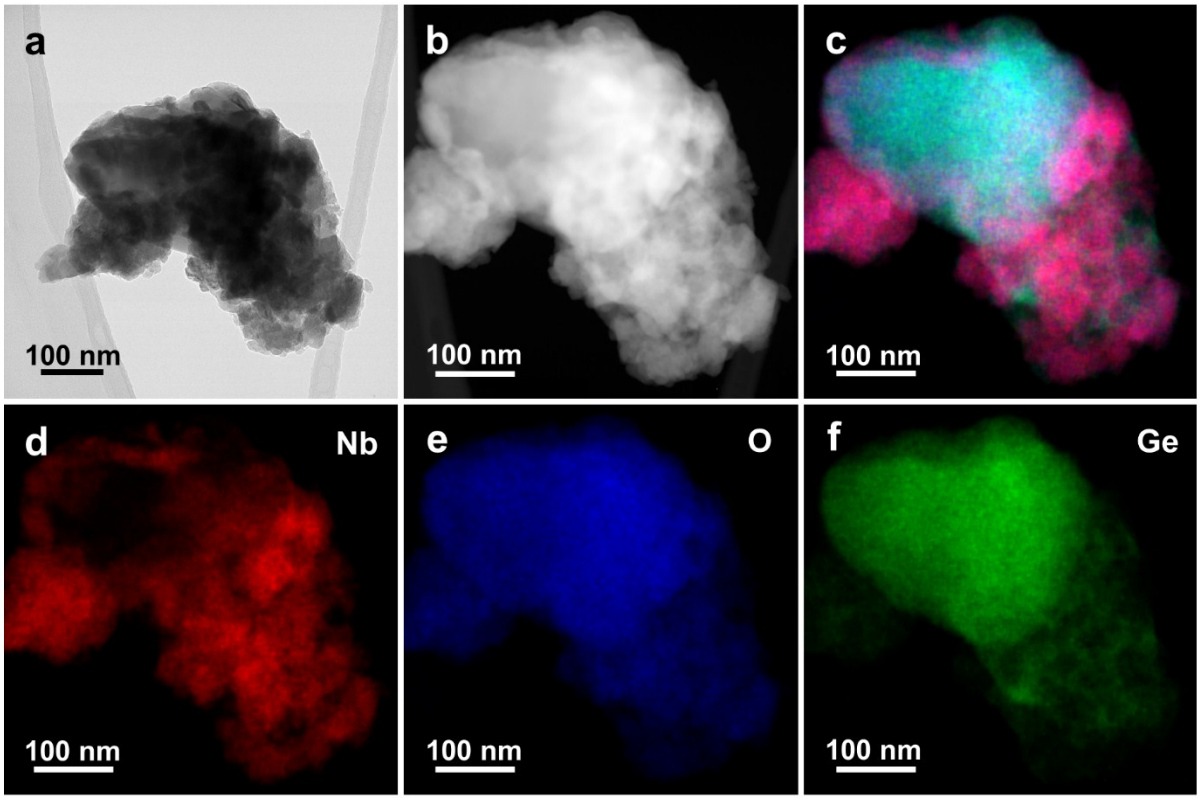

Fig. S8. (a) TEM image, (b) HAADF TEM image, and (c–f) EDS elemental mapping images of Nb_2O_5–Ge/GeO_2 cluster particles containing a saturated Ge precursor concentration (10 mmol).

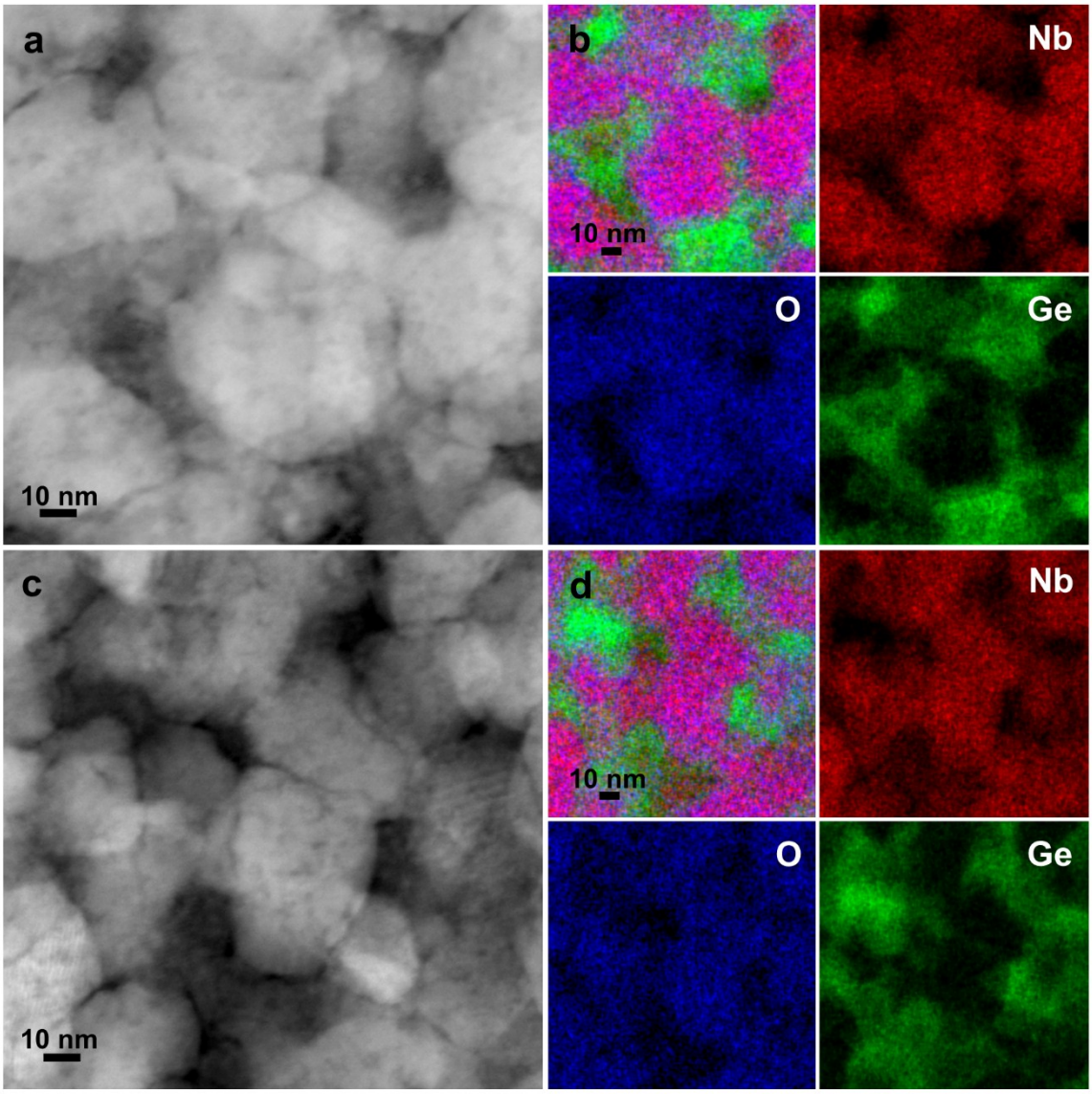

Fig. S9. High-magnification scanning transmission electron microscopy (STEM) images and EDS elemental mapping images corresponding to (a and b) S1 dash box and (c and d) S2 dash box in Figure 3a.

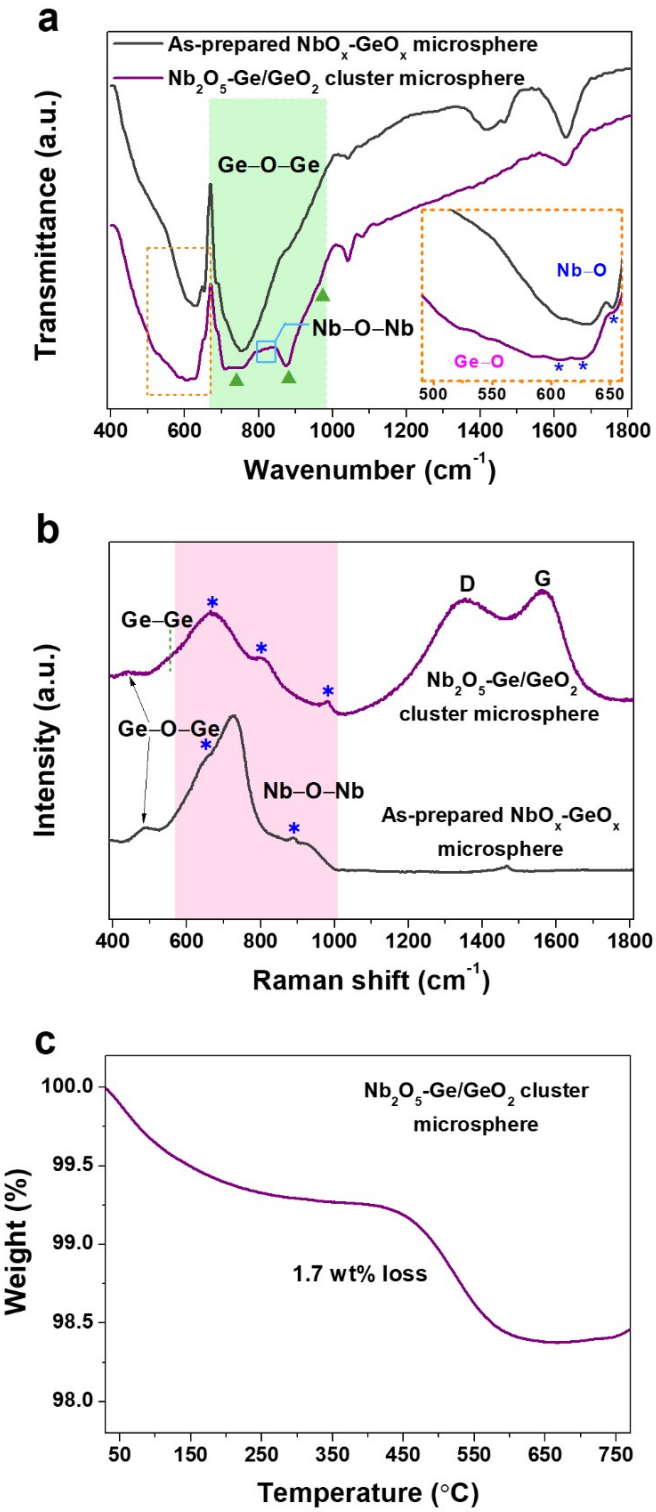

Fig. S10. (a) FT-IR and (b) Raman spectra of as-prepared NbO_x–GeO_x and annealed Nb_2O_5–Ge/GeO_2 cluster microspheres. (c) TGA curve of Nb_2O_5–Ge/GeO_2 cluster microspheres showing the content of pyrolyzed carbon after annealing.

Fig. S10a shows the FT-IR spectra of the as-prepared NbO_x–GeO_x and Nb_2O_5–Ge/GeO_2 cluster microspheres. The triplet at 515, 545, and 585 cm^{-1} in the case of the Nb_2O_5–Ge/GeO_2 cluster microspheres can be attributed to Ge–O antisymmetric stretching, which is related to the hexagonal crystal structure of GeO_2.[S1–3] The other three bands at 610, 625, and 650 cm^{-1} corresponded to Nb–O stretching [S4]. These can be observed as a signal mode of the distorted octahedra bond accompanying collinear Nb–O–Nb in T-Nb_2O_5.[S4] Strong transmittance signals were observed in the range 650–1000 cm^{-1}, which can be assigned to the Ge–O–Ge antisymmetric stretching mode. The sharp band at 880 cm^{-1} and the weak shoulder at 960 cm^{-1} corresponded to the vibration mode of GeO_4.[S1] All these features confirm the formation of niobium oxides and germanium oxides in the microspheres after annealing. Fig. S10b shows the Raman spectra of the as-prepared NbO_x–GeO_x and Nb_2O_5–Ge/GeO_2 cluster microspheres. Similar to the FT-IR results, characteristic features for niobium oxides and germanium oxides were observed.[S5,S6] It should be noted that the D and G bands at 1340 and 1595 cm^{-1}, respectively, were clearly observed in the Raman spectrum of the Nb_2O_5–Ge/GeO_2 cluster microspheres.[S7] These bands can be attributed to pyrolyzed carbon, which is generated from the PVP co-polymer during the annealing process.[S8] TGA experiments were performed to analyze the carbon content in the Nb_2O_5–Ge/GeO_2 cluster microspheres, the results of which are shown in Fig. S10c. The weight loss was measured to be approximately 1.7%, which would be the amount of pyrolyzed carbon in the microspheres.

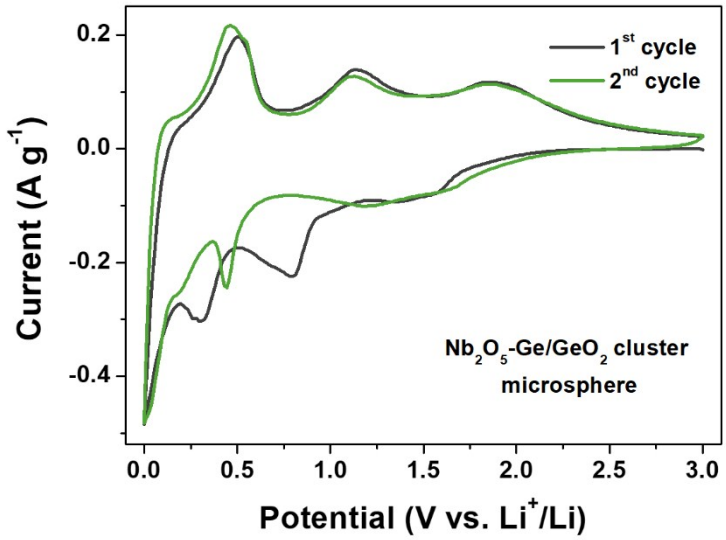

Fig. S11. CV curves of Nb_2O_5–Ge/GeO_2 cluster microsphere electrodes measured at a scan rate of 0.1 mV s^{-1} in the potential range of 0.001–3.0 V (vs. Li^+/Li).

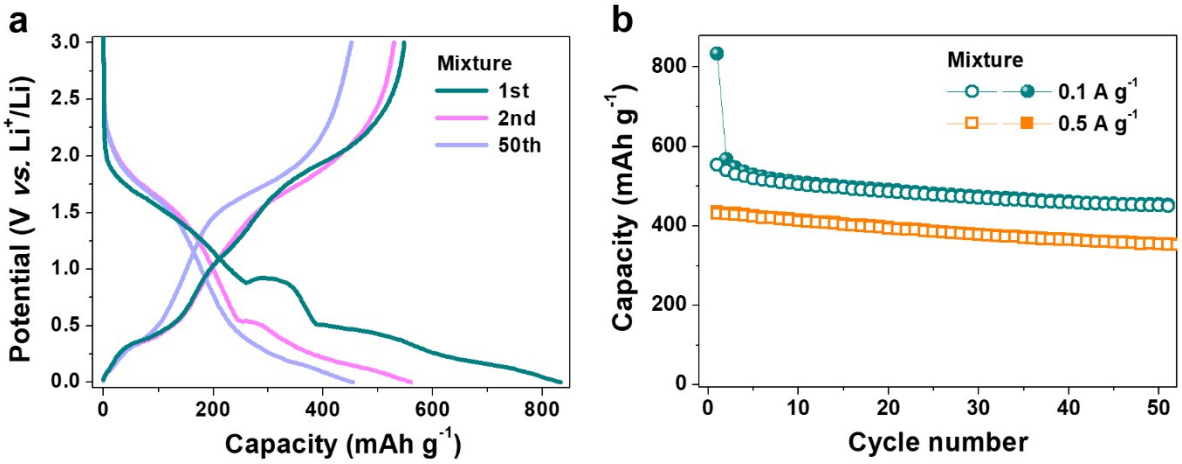

Fig. S12. (a) Voltage profiles for a mixed electrode (80 wt.% T-Nb_2O_5 and 20 wt.% GeO_2) with a current density of 0.1 A g^{-1} and (b) cyclic performance of the mixed electrode.

The ratio of T-Nb_2O_5 and GeO_2 was calculated based on the starting materials (precursors). It can be not very accurate because the ratio could be varied during the synthetic processes. However, the mixed electrode exhibited gradual capacity fading although it had lower capacities than those of the Nb_2O_5-Ge/GeO_2 cluster microsphere electrode. This indicates that the material design of cluster microspheres is effective for capacity retention.

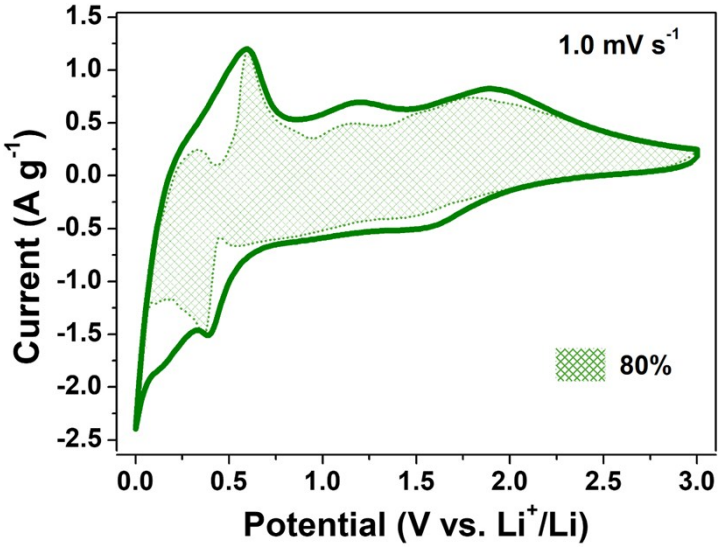

Fig. S13. CV curve with separation between the total current (solid line) and capacitive currents (shaded regions) at 1.0 mV s^{-1}.

Notes and references

S1. M. Winter and M. G. Kanatzidis, *Science*, 2006, **313**, 817–820.

S2. Y.-W. Chiu and M. H. Huang, *J. Phys. Chem. C*, 2009, **113**, 6056–6060.

S3. K. H. Seng, M.-H. Park, Z. P. Guo, H. K. Liu and J. Cho, *Nano Lett.*, 2013, **13**, 1230–1236.

S4. T. Ikeya and M. Senna, *J. Non-Cryst. Solids*, 1988, **105**, 243–250.

S5. T. P. Mernagh and L.-G. Liu, *Phys. Chem. Minerals*, 1997, **24**, 7–16.

S6. J.-M. Jehng and I. E. Wachs, *Chem. Mater.*, 1991, **3**, 100–107.

S7. Y. Z. Jin, C. Gao, W. K. Hsu, Y. Zhu, A. Huczko, M. Bystrzejewski, M. Roe, C. Y. Lee, S. Acquah, H. Kroto, and D. R. M. Walton, *Carbon*, 2005, **43**, 1944–1953.

S8. Z. Zhang, B. Zhao and L. Hu, *J. Solid State Chem.*, 1996, **121**, 105–110.